Spectroscopy of Yb^{3+},Ho^{3+},Eu^{3+}-codoped calcium niobium gallium garnet (CNGG) crystal

Xu Li[a], Kirill Eremeev[b], Pavel Loiko[b,*], Youshi Zhou[a], Yuxia Zhang[a], Junhai Liu[a], Zhongben Pan[c], Alain Braud[b], Jean-Louis Doualan[b], Sami Slimi[d], Rosa Maria Solé[d], Xavier Mateos[d,e], Patrice Camy[b], and Honghao Xu[a,f,**]

[a]*College of Physics, Qingdao University, Ning-xia Road 308, Qingdao, 266071, China*
[b]*Centre de Recherche sur les Ions, les Matériaux et la Photonique (CIMAP), UMR 6252 CEA-CNRS-ENSICAEN, Université de Caen Normandie, 6 Boulevard Maréchal Juin, 14050 Caen Cedex 4, France*
[c]*School of Information Science and Engineering, Shandong University, Qingdao, 266237, China*
[d]*Universitat Rovira i Virgili, Física i Cristal·lografia de Materials (FiCMA, Marcel·lí Domingo 1, 43007 Tarragona, Spain*
[e]*Serra Húnter fellow, Spain*
[f]*State Key laboratory of Crystal Material, Shandong University, Jinan 250100, PR China*
**Corresponding author, e-mail: pavel.loiko@ensicaen.fr*
***E-mail: xuhonghao@qdu.edu.cn*

Abstract: Calcium niobium gallium garnet (CNGG) crystals codoped with Yb^{3+}, Ho^{3+} and Eu^{3+} ions were grown by the Czochralski method. The crystal structure (cubic, sp. gr. O^{10}_h - *Ia*3*d*, lattice constant a = 12.4748(2) Å) was refined by the Rietveld method. A Raman study revealed high-energy vibrations at 767 – 846 cm^{-1} due to the [Nb2|$Ga2O_4$] groups. The spectroscopic properties of Yb,Ho: and Yb,Ho,Eu:CNGG crystals were studied with the goal of developing broadband emitting gain media around 2 μm and 3 μm. The maximum stimulated-emission cross-sections σ_{SE} are 0.57×10^{-20} cm^2 at 2070 nm (the $^5I_7 \rightarrow {}^5I_8$ Ho^{3+} transition) and 1.01×10^{-20} cm^2 at 2869 nm (the $^5I_6 \rightarrow {}^5I_7$ Ho^{3+} transition) and the emission spectra are smooth and broad owing to the structural disorder of the CNGG host matrix. The evidence of $Yb^{3+}(^2F_{5/2}) \rightarrow Ho^{3+}(^5I_6)$ energy transfer (ET) in the Yb,Ho:CNGG crystal is shown. Without Eu^{3+}, the luminescence lifetimes of the $^5I_6$ and $^5I_7$ Ho^{3+} states are 0.30 ms and 7.24 ms, respectively. The Eu^{3+} codoping leads to the quenching of the $^5I_7$ Ho^{3+} lifetime due to the $Ho^{3+}(^5I_7) \rightarrow Eu^{3+}(^7F_6)$ ET which is favorable for 3 μm laser operation. The crystal-field splitting of the Ho^{3+} multiplets is revealed at 12 K. First laser operation in Yb,Ho:CNGG crystals at 2.1 μm is achieved.

Keywords: garnet crystals; holmium ions; optical spectroscopy; luminescence; mid-infrared.

1. Introduction

Disordered calcium niobium gallium garnets (CNGG) are known as laser host media for doping with trivalent rare-earth ions (RE^{3+}) [1-3]. They belong to the family of cubic multicomponent garnets $\{A\}_3[B]_2(C)_3O_{12}$, where {}, [], and () stand for dodecahedral (Wyckoff: 24*c*), octahedral (16*a*), and tetrahedral (24*d*) sites, respectively. Stoichiometric CNGG has a chemical formula $\{Ca_3\}[Nb_{1.5}Ga_{0.5}](Ga_3)O_{12}$ [4] but the actual crystal composition deviates from the stoichiometry resulting in a distribution of both Ga^{3+} and Nb^{5+} cations over the [B] and (C) sites and a presence of cationic vacancies [5,6]. This determines the structure disorder. The dopant RE^{3+} ions substitute for the Ca^{2+} ones in {A} sites and their absorption and emission spectra exhibit significant inhomogeneous broadening owing to the possible different environments of local ligands [3]. Like other garnet compounds, CNGG crystals can be easily grown by the conventional Czochralski (Cz) method [2].

The broadband emission properties of RE^{3+} ions in CNGG crystals have attracted attention over the past few years for laser development. First studies mainly focused on Nd^{3+} and Yb^{3+} ions leading to emission around 1 μm [7-9]. More recently, the research focus shifted to CNGG-type crystals doped with Tm^{3+} and Ho^{3+} ions [10-14]. Such materials have been recognized as excellent gain media for broadly tunable and especially mode-locked lasers emitting around 2 μm capable of generating ultrashort pulses at this wavelength. Pan *et al.* reported on a Tm,Ho:CNGG laser delivering 413 mW at 2.088 μm and a continuous wavelength tuning between 1.94 – 2.144 μm [13]. A Tm^{3+},Ho^{3+},Li^{+}-codoped CNGG crystal was used to generate pulses as short as 67 fs at a central wavelength of 2.083 μm [14].

Holmium ions (Ho^{3+}, electronic configuration: $[Xe]4f^{10}$) are well known for their emission at 2.1 μm associated with the $^5I_7 \rightarrow {}^5I_8$ transition. Efficient and power scalable Ho lasers operating on this transition and employing resonant (in-band) pumping directly to the upper laser level ($^5I_7$) are known [15]. The Cz growth of Ho:CNGG crystals was reported by Shimamura et al. [16]. Ryabochkina *et al.* demonstrated an in-band-pumped Ho:CNGG laser delivering up to 2.1 W at 2.095 μm [17]. Spectral properties and laser performance of Ho:CNGG crystals grown by the micro-pulling-down method were studied in [18].

Apart from the direct excitation of Ho^{3+} ions, an Yb^{3+},Ho^{3+} codoping scheme is known [19]. It is based on excitation of Yb^{3+} ions featuring strong absorption at ~1 μm followed by energy-transfer, $^2F_{5/2}(Yb^{3+}) \rightarrow {}^5I_6(Ho^{3+})$. Yb^{3+} ions can be pumped by commercial InGaAs laser diodes. Laser operation of Yb^{3+},Ho^{3+}-codoped garnet crystals (such as YAG and YSGG) was reported [20-22]. Moreover, this scheme was also exploited in fiber lasers [23].

Less common but still very interesting is another Ho^{3+} transition, $^5I_6 \rightarrow {}^5I_7$, falling into the mid-infrared spectral range (2.9 μm) [24,25]. Laser sources emitting around this wavelength are of interest for spectroscopy, laser surgery, material processing and environmental monitoring. One of the difficulties for developing 2.9 μm Ho lasers is the self-terminating nature of this laser transition due to the longer lifetime of the lower laser level. It can be overcome by cascade lasing, $^5I_6 \rightarrow {}^5I_7 \rightarrow {}^5I_8$ [24], or by resonant excited-state absorption from the metastable $^5I_7$ level [25]. Another difficulty is the weak Ho^{3+} absorption to the $^5I_6$ state, so that efficient pumping is possible mainly in the fiber laser geometry.

The Yb^{3+},Ho^{3+} codoping scheme can eliminate the problem of the weak pump absorption opening the way towards laser operation in bulk crystals. Diening *et al.* proposed to add Eu^{3+} ions for an additional lifetime shortening of the terminal laser level for the $^5I_6 \rightarrow {}^5I_7$ transition and reported on the 2.9 μm laser operation in a triply codoped Yb,Ho,Eu:YSGG crystal [21]. The addition of Eu^{3+} and Tb^{3+} ions for the lifetime quenching of the lower-lying excited state of Tm^{3+} for releasing the limitation of the self-terminating laser transition was also studied by Braud *et al.* [26].

In the present paper, we report on the growth, structure and spectroscopic properties of Yb^{3+},Ho^{3+} and Yb^{3+},Ho^{3+},Eu^{3+} codoped CNGG crystals with the goal of developing materials with broadband emission properties around 2.1 μm and 2.9 μm. We also present the first laser operation of Yb,Ho:CNGG crystals on the $^5I_7 \rightarrow {}^5I_8$ transition.

2. Crystal growth

A series of Yb^{3+},Ho^{3+},Eu^{3+}-codoped calcium niobium gallium garnet crystals (shortly Yb,Ho,Eu:CNGG) was grown by the Czochralski (Cz) method, cf. Table 1 for the initial doping levels. We describe the growth of a 10 at.% Yb^{3+}, 1 at.% Ho^{3+}, 0.075 at.% Eu^{3+}-codoped crystal (nominal composition, the atomic fractions are indicated with respect to the Ca^{2+} cations). The starting materials, $CaCO_3$ (purity: 4N), Nb_2O_5 (4N), Ga_2O_3 (5N) and RE_2O_3 (RE = Yb, Ho, Eu, 5N) were weighed according to the following chemical formula:

$$3CaCO_3 + 0.84375Nb_2O_5 + 1.8875Ga_2O_3 + 0.15Yb_2O_3 + 0.015Ho_2O_3 + 0.01125Eu_2O_3 = Ca_3Nb_{1.6875}Ga_{3.1875}O_{12}\cdot 0.1Yb_3Ga_5O_{12}\cdot 0.01Ho_3Ga_5O_{12}\cdot 0.0075Eu_3Ga_5O_{12} + 3CO_2\uparrow.$$

To compensate the volatilization of Ga_2O_3 during the synthesis of the polycrystalline material and the crystal growth, an excess of 1.0 wt% Ga_2O_3 was added. The raw materials were first mixed during 24 h and heated at 1173 K in a Pt crucible for 10 h to decompose $CaCO_3$. After cooling to room temperature (RT, 293 K), the mixture was ground to powder, mixed for 24 h and pressed into pellets and reheated at 1373 K for 15 h to synthesize the Yb,Ho,Eu:CNGG polycrystalline material.

The growth process was performed with an Pt crucible at the air atmosphere. The seed was cut from an Yb:CNGG crystal along the [111] crystallographic direction. The pulling rate was 0.5 - 3.0 mm/h and the rotation speed was 5 - 20 revolutions per minute (rpm).

For comparison, we have also used two Yb^{3+},Ho^{3+}-codoped crystals (Table 1). The description of the crystal growth can be found elsewhere [27].

A photograph of an as-grown Yb,Ho,Eu:CNGG crystal boule is shown in Fig. 1. It has a cylindric shape with a uniform cross-section in the central part of the boule (diameter: 25 mm, length: 30 mm). The cross-section is circular, which is typical for the Cz method. The crystal boule is transparent and neither cracks nor inclusions are observed. The as-grown crystal shows a slight yellow coloration due to the absorption of color centers in the visible related to cationic vacancies, a typical behavior for CNGG-type crystals [12].

The actual concentrations of Yb^{3+} and Ho^{3+} ions were measured using the Inductively-Coupled Plasma Mass Spectrometry method (ICP-MS, Agilent), Table 1. The Eu^{3+} doping level was below the sensitivity limit of the used equipment. For the above-described crystal, the actual doping levels are 11.5 at.% Yb^{3+} and 1.25 at.% Ho^{3+} corresponding to the ion

densities N_{Yb} = 14.1×10^{20} cm^{-3} and N_{Ho} = 1.54×10^{20} cm^{-3}, respectively. The segregation coefficients for Yb^{3+} and Ho^{3+} ions, $K_{RE} = C_{crystal}/C_{melt}$, amount to 1.15 and 1.25, respectively. The determined K_{RE} values are almost independent of the initial crystal composition.

3. Experimental

The powder X-ray diffraction (XRD) measurements for the Rietveld refinement of the crystal structure were carried out using a Bruker-AXS D8-Advanced diffractometer equipped with a vertical θ-θ goniometer. The equipment had the incident and diffracted beam Soller slits of 2.5°, a fixed receiving slit of 0.5° and an air-scattering knife on the surface of the sample. The Cu Kα radiation was generated with a copper X-ray tube working at 40 kV and 40 mA. The sample was placed on a Si (510) support with low background. The measurements were performed with an angular step of 0.02° and a step time of 2 s. The X-ray diffraction pattern was recorded in the 2θ angular range of 15 - 90°. The diffracted X-rays were detected with a LynxEye-XE-T PSD detector, working with an opening angle of 2.94°.

The Raman spectra were measured using a confocal Raman microscope (Renishaw inVia) equipped with an × 50 objective and an Ar^+ ion laser (λ_{exc} = 457 nm).

The absorption spectra were measured using a spectrophotometer (Lambda 1050, Perkin Elmer). The IR luminescence spectra of Yb^{3+} and Ho^{3+} ions were measured using two optical spectrum analyzers (OSA): Ando AQ (at 0.9-1.3 μm) and Yokogawa AQ6376 (at 2.8 – 3.2 μm) using a Ti:Sapphire laser as an excitation source. To reduce the effect of water vapor absorption, the second OSA was purged with nitrogen. The luminescence and excitation spectra of Eu^{3+} ions in the visible were measured using a spectrofluorimeter (QuantaMaster).

For low-temperature (LT, 12 K) studies, the sample was mounted on an APD DE-202 closed-cycle cryo-cooler equipped with an APD HC 2 Helium vacuum cryo-compressor and a Laceshore 330 temperature controller.

The luminescence decay curves were measured using a ns optical parametric oscillator (OPO, Horizon, Continuum), a 1/4 m monochomator (Oriel 77200), a photomultiplier tube (in the visible) / an InGaAs detector (in the IR) and an 8 GHz digital oscilloscope (DSA70804B, Tektronix).

4. Results and discussion

4.1. Structural study

The phase purity and the crystal structure were confirmed by X-ray powder diffraction (XRD). The measured XRD pattern of the Yb,Ho,Eu:CNGG crystal (11.5 at.% Yb^{3+}, 1.25 at.% Ho^{3+}, 0.075 at.% Eu^{3+}) is shown in Fig. 2, together with the results of the structure refinement by the Rietveld method using the Match3 software (the crystal structure of undoped CNGG [5] was taken as a starting model). Only one phase with a cubic garnet structure (sp. gr. O^{10}_h - *Ia*3*d*, No. 230) is identified. The determined lattice constant a = 12.4748(2) Å, the volume of the unit-cell V = 1941.34(4) Å^3 (number of the formula units per unit-cell: Z = 2) and the calculated crystal density ρ_{calc} = 5.309 g/cm^3. The following

refinement *R*-factors were obtained: R_{exp} = 2.10% R_{wp} = 6.35%, and the reduced khi-squared $\chi^2 = (R_{wp}/R_{exp})^2 = 9.18$ indicating a relatively good convergence of the fit.

CNGG is an example of a multicomponent garnet with a general chemical formula $\{A\}_3[B]_2(C)_3O_{12}$. A stoichiometric CNGG crystal has a chemical formula $Ca_3Nb_{1.5}Ga_{3.5}O_{12} = \{Ca_3\}[Nb_{1.5}Ga_{0.5}](Ga_3)O_{12}$. For any real doped or undoped crystal, its composition deviates from the stoichiometry. The determined fractional atomic coordinates (*x*, *y*, *z*), the site occupancy factors (O.F.) and the isotropic displacement parameters (B_{iso}) for the Yb,Ho,Eu:CNGG crystal are listed in Table 2. The dodecahedral sites are occupied by the Ca^{2+} and $Yb^{3+}|Ho^{3+}|Eu^{3+}$ cations (the corresponding O.F. were taken according to the results of the ICP-MS analysis, cf. Table 1). The Ga^{3+} and Nb^{5+} cations are randomly distributed over two non-equivalent sites (the octahedral and tetrahedral ones, respectively) which determines the structure disorder.

According to the determined atomic coordinates, we draw a fragment of the crystal structure, Fig. 3. The unit-cell of Yb,Ho,Eu:CNGG contains 160 atoms. The dodecahedral {A} sites are occupied by Ca^{2+} and RE^{3+} ions. When the dopant RE^{3+} ions are incorporated into the CNGG lattice, they are supposed to replace for the Ca^{2+} ones because of the closeness of the corresponding ionic radii for VIII-fold oxygen coordination (R_{Yb} = 0.985 Å, R_{Ho} = 1.015 Å, and R_{Eu} = 1.066 Å, compared with R_{Ca} = 1.12 Å). There are 4 shorter (2.3932(9) Å) and four longer (2.5179(8) Å) interatomic distances in the $[Ca|REO_8]$ polyhedra indicating a distorted dodecahedral coordination. For the $[Nb1|Ga1O_6]$ and $[Nb2|Ga2O_4]$ polyhedra, the metal-oxygen interatomic distances are 1.9960(2) Å (×6) and 1.8547(8) Å (×4), respectively. In the CNGG structure, each $[Nb1|Ga1O_6]$ octahedron is connected with six $[Nb2|Ga2O_4]$ tetrahedra, and each $[Nb2|Ga2O_4]$ tetrahedron is connected with four $[Nb1|Ga1O_6]$ octahedra, and these polyhedra are linked by corner-sharing, which results in the formation of a dodecahedron void, Fig. 3. The $Ca^{2+}|RE^{3+}$ cations occupy the centers of these voids.

The vibrational properties of Yb,Ho: and Yb,Ho,Eu:CNGG crystals were studied by Raman spectroscopy, Fig. 4. In the range of frequencies from 700 to 900 cm^{-1}, the Raman spectra of CNGG-type crystals show two groups of vibrations usually assigned to symmetric stretching modes (ν_s) of isolated metal-oxygen tetrahedra $[M2O_4]$. The tetrahedral M2 sites are occupied by both Nb^{5+} and Ga^{3+} cations. The peaks at higher frequencies are related to the $[Nb2O_4]$ groups and those at lower frequencies – to the $[Ga2O_4]$ ones [1,6]. There are two peaks at 827 cm^{-1} (C_4, undistorted $[Nb2O_4]$ terahedra) and 846 cm^{-1} (C_5, vacancies) and two other peaks at 787 cm^{-1} (C_2, undistorted $[Ga2O_4]$ tetrahedra) and 767 cm^{-1} (C_1, vacancies). The structural distortion of the $[M2O_4]$ tetrahedra is evidenced by the appearance of satellite peaks due to a nearby cationic vacant position. However, the relative intensity of the satellite C_5 and C_1 peaks is weak indicating a moderate distortion of the $[M2O_4]$ tetrahedra. The Raman spectra are weakly dependent on the concentration of Ho^{3+} and Eu^{3+} ions which are relatively low compared to the Yb^{3+} concentration. Compared to undoped CNGG crystals (C_4 = 832 cm^{-1}, C_2 = 763 cm^{-1}), the heavy Yb^{3+} doping induces a frequency shift for both the C_4 and C_2 characteristic peaks.

4.2. Optical absorption

The absorption spectra of two CNGG crystals both codoped with 11.5 at.% Yb^{3+}, 1.25 at.% Ho^{3+} and containing no Eu^{3+} or 0.075 at.% Eu^{3+} are shown in Fig. 5.

The most intense absorption band at ~1 μm is related to the $^2F_{7/2} \rightarrow {}^2F_{5/2}$ transition of Yb^{3+} ions. The narrow peak at 972.2 nm corresponding to the zero-phonon-line (ZPL) has a bandwidth (full width at half maximum, FWHM) of 2.9 nm and the peak absorption cross-section $\sigma_{abs} = 1.48\times10^{-20}$ cm^2. At shorter wavelengths, several overlapping broad peaks with maxima at 944.0, 933.4, 927.8 and 920.9 nm appear. The corresponding σ_{abs} is in the range of $0.48 – 0.60\times10^{-20}$ cm^2.

The absorption spectrum also contains multiple bands assigned to Ho^{3+} transitions from the ground-state ($^5I_8$) to the excited-states ranging from $^5I_7$ to $^3K_6$. Here, the assignment is according to Carnall *et al*. [28]. In particular, the broad absorption band spanning from 1.82 to 2.12 μm is related to the $^5I_8 \rightarrow {}^5I_7$ Ho^{3+} transition. The maximum absorption cross-section for this transition $\sigma_{abs} = 0.51\times10^{-20}$ cm^2 lies at 1918 nm.

A careful comparison of the absorption spectra of the crystals with and without Eu^{3+} reveals its spectroscopic signatures. The band in the blue (394 nm) corresponds to the $^7F_{0,1} \rightarrow {}^5L_6$ transition, Fig. 5(a), and a rise of the absorption intensity at 2 – 2.2 μm – to the $^7F_{0,1} \rightarrow {}^7F_6$ one, Fig. 5(c). This indicates the possibility of the $Ho^{3+}(^5I_7) \rightarrow Eu^{3+}(^5F_6)$ energy transfer.

4.3. Emission (spectra and lifetimes)

The luminescence spectra of Yb^{3+} and Ho^{3+} ions in the CNGG crystal were measured under excitation at 972 nm (to the $^2F_{5/2}$ Yb^{3+} manifold) as shown in Fig. 6. Figure 7 shows a scheme of energy-levels of Yb^{3+}, Ho^{3+} and Eu^{3+} ions indicating the relevant spectroscopic processes for the emissions of these species.

Yb^{3+} ions exhibit a broad emission band spanning from 0.9 to 1.1 μm related to the $^2F_{5/2} \rightarrow {}^2F_{7/2}$ transition with a maximum at 1027 nm, Fig. 6(a). The narrow peak at 972.2 nm is related to the ZPL transition in emission.

Three Ho^{3+} emission bands in the IR are observed. The emissions at 1.11 – 1.25 μm with a maximum at 1202 nm and at 2.65 – 3.15 μm with a maximum at 2868 nm originate from transitions from the $^5I_6$ intermediate level to the ground-state ($^5I_8$) and the first excited-state ($^5I_7$), respectively, Fig. 6(b,d). This manifold is populated by a phonon-assisted energy-transfer process, Yb^{3+} ($^2F_{5/2}$) → $Ho^{3+}(^5I_6)$. The emission at 1.8 – 2.25 μm with a maximum at 2069 nm originates from transitions from the metastable Ho^{3+} level ($^5I_7$) to the ground-state ($^5I_8$), Fig. 6(c).

The luminescence spectra are smooth and broad due to a significant inhomogeneous spectral broadening for the dopant rare-earth ions (Yb^{3+} and Ho^{3+}) owing to the disordered nature of the CNGG host matrix. The shape of the luminescence spectra of Ho^{3+} ions does not depend on the Eu^{3+} codoping. The intensity of Ho^{3+} luminescence at ~2 μm (the $^5I_7 \rightarrow {}^5I_8$ transition) notably decreases upon the presence of Eu^{3+}, Fig. 6(c), due to its quenching effect on the $^5I_7$ Ho^{3+} manifold. A certain reduction of the luminescence intensity for Eu^{3+}-containing crystals is also observed at ~2.9 μm (the $^5I_6 \rightarrow {}^5I_7$ transition), Fig. 6(d), but it is

much weaker than in the former case. These observations are in line with lifetime measurements (see below).

The luminescence spectra of Eu^{3+} ions in the codoped CNGG crystals are shown in Fig. 8(a), measured under excitation in the blue at 395 nm (to the $^5L_6$ manifold). They contain several bands peaking at 579, 588-594, 610, 653 and 706 nm related to transitions from the metastable state $^5D_0$ to the group of closely located ^7F_J states (where J = 0...4, respectively, $^7F_0$ being the Eu^{3+} ground-state). The most intense emission band at 610 nm is due to the $^5D_0 \rightarrow {}^7F_2$ transition and it determines the red color of Eu^{3+} luminescence. The emission bands are also inhomogeneously broadened.

The emission properties of Eu^{3+} ions are known to be sensitive to the site symmetry and its distortion and can be considered as a "structural probe". In particular, the ratio of integrated intensities of the purely electric-dipole (ED) $^5D_0 \rightarrow {}^7F_2$ transition and the purely magnetic-dipole (MD) $^5D_0 \rightarrow {}^7F_1$ one, called the asymmetry parameter, R, for Eu^{3+} ions in CNGG is determined to be 2.45. The R value well above 1 indicates that the Eu^{3+} sites have no center of inversion. This agrees with the structural analysis: the Eu^{3+} ions are expected to replace Ca^{2+} cations in sites with a local symmetry D_2 or lower. Another interesting feature of Eu^{3+} ions is the $^5D_0 \rightarrow {}^7F_0$ transition which is both ED and MD forbidden. For the studied crystals, only one peak at 579.44 nm (17258 cm^{-1}) is observed in line with a single type of sites for rare-earth ions in CNGG. However, this peak is notably broadened as compared to ordered crystals. This was previously explained by the different ways of arrangements of Nb^{5+} and Ga^{3+} in the nearest to Eu^{3+} tetrahedral and octahedral nodes of the lattice [29].

The excitation spectra for Eu^{3+} ions were also measured, Fig. 8(b). It contains bands related to transitions from the $^7F_{0,1}$ states to different excited-states: $^5D_0$ (~579 nm), $^5D_1$ (~526 nm), $^5D_2$ (~464 nm), $^5D_3$ (416 nm) and $^5L_6$ (394 nm). At shorter wavelengths, the assignment of the absorption peaks is complicated due to the overlapping of several higher-lying ^5L_J, ^5H_J and ^5G_J multiplets. The most intense band in the excitation spectrum centered at 394 nm corresponds to transitions to the $^5L_6$ state in agreement with the absorption spectrum, Fig. 5(a).

Note that no Eu^{2+} signatures are observed in the spectra.

The stimulated-emission (SE) cross-sections, σ_{SE}, for transitions of Ho^{3+} ions in the near- and mid-IR were calculated using two methods. The first one is the Füchtbauer-Ladenburg (F-L) formula [30]:

$$\sigma_{SE}(\lambda) = \frac{\lambda^5}{8\pi < n >^2 \tau_{rad} c} \frac{B(JJ')W'(\lambda)}{\int \lambda W'(\lambda) d\lambda}, , \quad (1)$$

where λ is the light wavelength, $<n>$ is the refractive index of the crystal at the mean emission wavelength calculated using the dispersion data from [6], τ_{rad} is the radiative lifetime of the emitting state and B(JJ') is the luminescence branching ratio (both taken from the Judd-Ofelt calculations for Ho^{3+} ions in CNGG [12]), c is the speed of light, and $W'(\lambda)$ is the measured luminescence spectrum corrected for the response of the set-up.

The second approach is based on the reciprocity method (RM) [31]:

$$\sigma_{SE}(\lambda) = \sigma_{abs}(\lambda) \frac{Z_1}{Z_2} \exp\left(-\frac{hc/\lambda - E_{ZPL}}{kT} \right), \quad (2)$$

where σ_{abs} is the absorption cross-section, h is the Planck constant, k is the Boltzmann constant, T is the crystal temperature (RT), E_{ZPL} is the ZPL energy corresponding to transitions between the lowest Stark sub-levels of the two multiplets, and Z_m are the partition functions of the lower (m = 1) and upper (m = 2) manifolds. Due to the impossibility to fully resolve the crystal-field splitting for Ho^{3+} ions in CNGG (see below), the crystal-field data of another Ho^{3+} doped gallium garnet, Ho:YGG [32], were used.

For the $^5I_6 \rightarrow {}^5I_8$ quasi-three-level Ho^{3+} transition, the maximum SE cross-section is 0.46×10^{-20} cm^2 at 1202 nm, as calculated by the F-L formula using $\tau_{rad}(^5I_6)$ = 3.69 ms and B(JJ') = 81.7%, Fig. 9(a). This value agrees very well with that obtained via the RM.

For the $^5I_7 \rightarrow {}^5I_8$ quasi-three-level Ho^{3+} transition interesting for laser operation slightly above 2 μm, the maximum σ_{SE} is 0.57×10^{-20} cm^2 at 2070 nm and another intense peak appears at a slightly longer wavelength with $\sigma_{SE} = 0.54\times10^{-20}$ cm^2 at 2082 nm, as calculated using the F-L formula with $\tau_{rad}(^5I_7)$ = 8.41 ms, Fig. 9(b). Again, a reasonable agreement with the RM is observed considering the effect of reabsorption on the measured luminescence spectrum visible at shorter wavelengths. The emission bandwidth (FWHM) of the band at ~2.08 μm is as broad as 83 nm.

For the mid-infrared emission interesting for laser operation at ~3 μm owing to the quasi-four-level $^5I_6 \rightarrow {}^5I_7$ Ho^{3+} transition, the maximum σ_{SE} is 1.01×10^{-20} cm^2 at 2869 nm and at longer wavelengths another two peaks appear at 2910 and 2920 nm corresponding to $\sigma_{SE} = 0.78\times10^{-20}$ cm^2, Fig. 9(c). Here, the calculated value is based on the F-L formula with $\tau_{rad}(^5I_6)$ = 3.69 ms and B(JJ') = 18.3%.

For the luminescence dynamics studies, the crystal samples were finely powdered to avoid the effect of reabsorption (luminescence trapping) on the measured lifetimes. The measured luminescence decay curves for the metastable states of Yb^{3+}, Ho^{3+} and Eu^{3+} ions are shown in Fig. 10 and the corresponding mean luminescence lifetimes τ_{lum} are given in Table 3. For Yb^{3+} ions, the decay from the $^2F_{5/2}$ excited-state was studied. For singly Yb^{3+}-doped CNGG studied for comparison, $\tau_{lum,0}$ = 0.978 ms. For Ho^{3+} codoping with an increased Ho^{3+} content, the $^2F_{5/2}$ lifetime is shortened due to the enhanced efficiency of the $Yb^{3+}(^2F_{5/2}) \rightarrow Ho^{3+}(^5I_6)$ energy-transfer. For 11.5 at.% Yb^{3+}, 1.25 at.% Ho^{3+}, the latter could be estimated as $\eta_{ET} \approx 1 - \tau_{lum}(Yb,Ho)/\tau_{lum,0}(Yb)$ = 46.5%. For the same doping levels of Yb^{3+} and Ho^{3+}, the addition of Eu^{3+} seems to slightly shorten the Yb^{3+} luminescence lifetime. This may indicate a possible process of a cooperative energy-transfer, $2Yb^{3+} \rightarrow Eu^{3+}$, involving pairs of excited Yb^{3+} ions [33]. The Yb^{3+} luminescence decay curves for all the samples with Ho^{3+} deviate from the single-exponential law.

For Ho^{3+} ions, the luminescence decay from the two lowest lying excited-states, $^5I_6$ and $^5I_7$, was studied under Yb^{3+} excitation. Because of this, the measured kinetics contain both the luminescence rise and decay. The rise time agrees with the lifetime of the $^2F_{5/2}$ Yb^{3+} state. For the Yb^{3+},Ho^{3+} codoped crystals (without Eu^{3+}), the $^5I_6$ and $^5I_7$ Ho^{3+} lifetimes are weakly dependent on the Ho^{3+} content in the range 0.94 – 1.25 at.% and amount to 0.30 ms and 7.24 ms, respectively. With adding Eu^{3+}, the $^5I_7$ Ho^{3+} lifetime is notably quenched as it amounts only to 3.24 ms for the sample with 1.25 at.% Ho^{3+} and 0.2 at.% Eu^{3+}. This is because of the $Ho^{3+}(^5I_7) \rightarrow Eu^{3+}(^7F_6)$ energy transfer promoted by the resonant location of the corresponding

manifolds of the two ions, followed by multiple non-radiative relaxation steps in the system of closely located lower-lying ^7F_J (J = 0 – 6) Eu^{3+} multiplets. The efficiency of this ET process can be estimated as $\eta_{ET} \approx 1 - \tau_{lum}(Ho,Eu)/\tau_{lum,0}(Ho) = 55.2\%$. Note that even a small addition of Eu^{3+} ions (0.2 at.%) is enough to induce a significant effect on the $^5I_7$ Ho^{3+} lifetime as the absorption cross-sections for the spin-allowed $^7F_{0,1} \rightarrow {}^7F_6$ Eu^{3+} transitions are relatively high compared to spin-forbidden transitions of Eu^{3+} in the visible spectral range. With Eu^{3+} addition, the lifetime of the $^5I_6$ Ho^{3+} level is also quenched but this effect is much weaker than for its $^5I_7$ counterpart. The lifetime reduction for Ho^{3+} ions upon Eu^{3+} codoping explains the drop in the luminescence intensity from these manifolds as shown in Fig. 6(b-d). Thus, the addition of Eu^{3+} is beneficial for potential laser operation of Yb,Ho,Eu:CNGG crystals at 2.9 μm as it helps to balance the lifetimes of the upper and lower laser levels.

For the Eu^{3+} ions, the lifetime of the metastable $^5D_0$ state was measured under excitation to the higher-lying $^5L_6$ manifold, Fig. 6(d). The luminescence decay curve deviates from a single-exponential law probably due to $Eu^{3+} \rightarrow Ho^{3+}$ and $Eu^{3+} \rightarrow 2Yb^{3+}$ energy-transfers. The mean luminescence lifetime $<\tau_{lum}>$ amounts to 0.90 – 0.92 ms.

4.4. Low-temperature spectroscopy

The spectroscopic properties of Ho^{3+} ions were studied at LT to resolve the crystal-field splitting of the multiplets involved in the studied near- and mid-IR emissions. The LT absorption spectra for the $^5I_8 \rightarrow {}^5I_7$ and $^5I_6$ transitions are shown in Fig. 11(a,b) giving access to the splitting of the $^5I_7$ and $^5I_6$ excited-states. The LT luminescence spectra for the $^5I_6 \rightarrow {}^5I_8$ and $^5I_7 \rightarrow {}^5I_8$ are shown in Fig. 11(c). Both of them are plotted vs. (photon energy – E_{ZPL}) thus directly giving access to the splitting of the ground-state, $^5I_8$. For the assignment of electronic transitions for Ho^{3+} ions in CNGG, we used the crystal-field data for Ho^{3+} ions in the isostructural YGG garnet [32]. The vertical dashes in Fig. 11 mark the positions of electronic transitions for this reference crystal.

Even at 12 K, the absorption and luminescence spectra of Ho^{3+} ions in CNGG are rather broad revealing a significant inhomogeneous spectral broadening. Note that almost no effect of the excitation wavelength on the measured LT emission spectra was observed. An attempt to determine the energies of individual Stark sub-levels for the $^5I_8$, $^5I_7$ and $^5I_6$ Ho^{3+} multiplets was made, cf. Table 4. It was assumed that each $^{2S+1}L_J$ multiplet is split into 2J + 1 sub-levels. Still, some experimental energy-levels are missing in Table 4.

The joint analysis of LT absorption and luminescence spectra as shown in Fig. 11(a) allowed us to determine the positions of the ZPL for the $^5I_8 \rightarrow {}^5I_7$ and $^5I_6$ transitions, namely E_{ZPL} = 5408 cm^{-1} ($^5I_8 \rightarrow {}^5I_7$) and E_{ZPL} = 8913 cm^{-1} ($^5I_8 \rightarrow {}^5I_6$). These values were used for calculating the SE cross-sections via the RM (see above).

4.5. Laser operation

The laser operation of the Yb,Ho:CNGG crystal on the $^5I_7 \rightarrow {}^5I_8$ Ho^{3+} transition was studied. The crystal codoped with 11.5 at.% Yb^{3+}, 1.25 at.% Ho^{3+} was used. A rectangular sample (thickness: 5.5 mm, aperture: 3.0×3.0 mm^2) was cut along the [111] crystallographic axis. It was double-side polished and left uncoated. The laser crystal was mounted on a Cu-

holder using a silver paint for better heat removal. A hemispherical laser cavity was used. It was formed by a flat dichroic mirror coated for high transmission (T = 92.5%) at 0.95 μm and high reflection (HR) at 1.85 – 2.3 μm and a set of concave output couplers (OCs) having a radius of curvature of -100 mm and a transmission T_{OC} in the range of 0.5% - 10% at 1.95 – 2.1 μm. The crystal was placed near the dichroic mirror with ~1 mm airgap. The cavity length was ~100 mm. The pump source was a Ti:Sapphire laser (3900S, Spectra Physics) emitting up to 2.5 W at 950 nm with a nearly diffraction limited beam (M^2 ~ 1). The pump radiation was focused into the crystal using an AR-coated lens (f = 75 mm). The pumping was in single pass. The measured pump absorption under lasing conditions was 71.2%. The residual pump was filtered out using a long-pass filter (LP1400, Spectrogon).

The input-output dependences of the Yb,Ho:CNGG laser are shown in Fig. 12(a). The laser generated a maximum output power of 19 mW at 2083-2089 nm with a slope efficiency η of 1.8% (with respect to the absorbed pump power) and a laser threshold of 0.52 W (for T_{OC} = 5%). With increasing the output coupling, the laser threshold gradually increased from 0.29 W (T_{OC} = 0.5%) to 0.63 W (T_{OC} = 10%). The input-output dependences were linear in the studied range of pump powers.

The typical spectra of the laser emission are shown in Fig. 12(b). The laser operated at ~2.09 μm (the $^5I_7 \rightarrow {}^5I_8$ Ho^{3+} transition) and the spectra experienced a slight blue shift with increasing the output coupling, from 2083 – 2099 nm (T_{OC} = 0.5%) to 2082 – 2087 nm (T_{OC} = 10%). This behavior is typical for quasi-three-level Ho lasers with intrinsic reabsorption. The laser emission was unpolarized. A typical oscilloscope trace of Ho^{3+} laser emission is shown in Fig. 12(c). The CW laser exhibits relaxation oscillations typical for ~2 μm Tm^{3+} and Ho^{3+} lasers. The laser operated on the fundamental transverse mode.

5. Conclusions

To conclude, Yb^{3+},Ho^{3+} and Yb^{3+},Ho^{3+},Eu^{3+} codoped CNGG crystals are attractive as broadband gain media for laser emitting at 2.1 μm (the $^5I_7 \rightarrow {}^5I_8$ Ho^{3+} transition) and 2.9 μm (the $^5I_6 \rightarrow {}^5I_7$ Ho^{3+} transition). A significant inhomogeneous broadening of absorption and emission bands of rare-earth ions in these crystals well preserved even at low temperatures (12 K) is due to the structure disorder originating from a random distribution of Ga^{3+} and Nb^{5+} cations over two different lattice sites, octahedral (16*a*) and tetrahedral (24*d*) ones. The Ho^{3+} ions in CNGG crystals exhibit relatively long luminescence lifetimes of the two lowest excited-states interesting for laser operation, namely 7.24 ms ($^5I_7$) and 0.30 ms ($^5I_6$). The Yb^{3+},Ho^{3+} codoping promotes the $Yb^{3+}(^2F_{5/2}) \rightarrow Ho^{3+}(^5I_6)$ energy transfer but its efficiency ($\eta_{ET} \approx$ 46.5% for 11.5 at.% Yb^{3+}, 1.25 Ho^{3+}) can be further optimized by adjusting the Yb^{3+}/Ho^{3+} ratio. The Eu^{3+} codoping leads to the quenching of the $^5I_7$ Ho^{3+} lifetime due to the $Ho^{3+}(^5I_7) \rightarrow Eu^{3+}(^7F_6)$ energy-transfer followed by multiphonon non-radiative relaxation between the group of closely located ^7F_J (J = 0 – 6) Eu^{3+} manifolds which is favorable for laser operation on the $^5I_6 \rightarrow {}^5I_7$ Ho^{3+} transition impaired by its self-terminating nature.

We report on the first laser operation of an Yb^{3+},Ho^{3+} codoped CNGG crystal at 2.1 μm (the $^5I_7 \rightarrow {}^5I_8$ Ho^{3+} transition): pumping at 950 nm, a maximum continuous-wave output power of 19 mW is achieved at 2083-2089 nm with a laser threshold of 0.52 W. Further

power scaling is expected via (i) optimizing the Yb^{3+}/Ho^{3+} codoping ratio for better $Yb^{3+} \rightarrow Ho^{3+}$ ET and (ii) using diode-pumping.

Acknowledgements

National Natural Foundation of China (Projects No. 51602166 and 52072351). Natural Science Foundation of Shandong Province, China (Grant ZR2022ME125) and Opening Project of State Key Laboratory of Crystal Material (NO. KF2210). "NOVAMAT" European project, co-funded by the Normandy County Council and the European Union in the framework of the ERDF-ESF operational program 2014-2020. "RELANCE" Chair of Excellence project funded by the Normandy Region. Grant PID2019-108543RB-I00 funded by MCIN/AEI/ 10.13039/501100011033. This research article has been possible with the support of the Secretaria d'Universitats I Recerca del Departament d'Empresa i Coneixement de la Generalitat de Catalunya, the European Union (UE), and the European Social Fund (ESF) (2021 FI_B1 00170).

References

1. Yu. K. Voronko, A. A. Sobol, A. Y. Karasik, N. A. Eskov, P. A. Rabochkina, S. N. Ushakov, Calcium niobium gallium and calcium lithium niobium gallium garnets doped with rare earth ions – effective laser media, Opt. Mater. 20 (2002) 197-209.
2. K. Shimamura, M. Timoshechkin, T. Sasaki, K. Hoshikawa, T. Fukuda, Growth and characterization of calcium niobium gallium garnet (CNGG) single crystals for laser applications, J. Cryst. Growth 128 (1993) 1021-1024.
3. Z. Pan, J. M. Serres, E. Kifle, P. Loiko, H. Yuan, X. Dai, H. Cai, M. Aguiló, F. Díaz, Y. Wang, Y. Zhao, U. Griebner, V. Petrov, X. Mateos, Comparative study of the spectroscopic and laser properties of Tm^{3+}, $Na^{+}(Li^{+})$-codoped $Ca_3Nb_{1.5}Ga_{3.5}O_{12}$-type disordered garnet crystals for mode-locked lasers, Opt. Mater. Express 8 (2018) 2287-2299.
4. Yu. K. Voron'ko, A. B. Kudryavtsev, N. A. Es'kov, V. V. Osiko, A. A. Sobol', E. V. Sorokin, and F. M. Spiridonov, Raman scattering of light in crystals and melt of calcium-niobium gallium garnet, Sov. Phys. Dokl. 32 (1998) 70-73.
5. E. Castellano-Hernández, M. D. Serrano, R. J. Jiménez Riobóo, C. Cascales, C. Zaldo, A. Jezowski, P. A. Loiko, Na modification of lanthanide doped $Ca_3Nb_{1.5}Ga_{3.5}O_{12}$-type laser garnets: Czochralski crystal growth and characterization, Cryst. Growth Des. 16 (2016) 1480-1491.
6. M. D. Serrano, J. O. Álvarez-Pérez, C. Zaldo, J. Sanz, I. Sobrados, J. A. Alonso, C. Cascales, M. T. Fernández-Díaz, A. Jezowski, Design of Yb^{3+} optical bandwidths by crystallographic modification of disordered calcium niobium gallium laser garnets, J. Mater. Chem. C 5 (2017) 11481-11495.
7. A. Lupei, V. Lupei, L. Gheorghe, L. Rogobete, E. Osiac, A. Petraru, The nature of nonequivalent Nd^{3+} centers in CNGG and CLNGG, Opt. Mater. 16 (2001) 403-411.
8. A. Schmidt, U. Griebner, H. Zhang, J. Wang, M. Jiang, J. Liu, V. Petrov, Passive mode-locking of the Yb:CNGG laser, Opt. Commun. 283 (2010) 567-569.
9. J.M. Serres, V. Jambunathan, P. Loiko, X. Mateos, H. Yu, H. Zhang, J. Liu, A. Lucianetti, T. Mocek, K. Yumashev, U. Griebner, V. Petrov, M. Aguiló, F. Díaz, Microchip laser operation of Yb-doped gallium garnets, Opt. Mater. Express 6 (2016) 46-57.

10. Y. Wang, Y. Zhao, Z. Pan, J. E. Bae, S. Y. Choi, F. Rotermund, P. Loiko, J. M. Serres, X. Mateos, H. Yu, H. Zhang, M. Mero, U. Griebner, V. Petrov, 78 fs SWCNT-SA mode-locked Tm:CLNGG disordered garnet crystal laser at 2017 nm, Opt. Lett. 43 (2018) 4268-4271.
11. Z. Pan, Y. Wang, Y. Zhao, H. Yuan, X. Dai, H. Cai, J. E. Bae, S. Y. Choi, F. Rotermund, X. Mateos, J. M. Serres, P. Loiko, U. Griebner, V. Petrov, Generation of 84-fs pulses from a mode-locked Tm:CNNGG disordered garnet crystal laser, Photon. Res. 6 (2018) 800-804.
12. Z. Pan, P. Loiko, Y. Wang, Y. Zhao, H. Yuan, X. Dai, H. Cai, J. M. Serres, S. Slimi, E. Dunina, A. Kornienko, J.-L. Doualan, P. Camy, U. Griebner, V. Petrov, M. Aguiló, F. Díaz, X. Mateos, Disordered Tm^{3+},Ho^{3+}-codoped CNGG garnet crystal: Towards efficient laser materials for ultrashort pulse generation at ~2 μm, J. Alloys Compd. 853 (2021) 157100-1-15.
13. Z. Pan, Y. Wang, Y. Zhao, M. Kowalczyk, J. Sotor, H. Yuan, Y. Zhang, X. Dai, H. Cai, J. E. Bae, S. Y. Choi, F. Rotermund, P. Loiko, J. M. Serres, X. Mateos, U. Griebner, V. Petrov, Sub-80 fs mode-locked Tm,Ho-codoped disordered garnet crystal oscillator operating at 2081 nm, Opt. Lett. 43 (2018) 5154-5157.
14. Y. Zhao, Y. Wang, W. Chen, Z. Pan, L. Wang, X. Dai, H. Yuan, Y. Zhang, H. Cai, J. E. Bae, S. Y. Choi, F. Rotermund, P. Loiko, J.M. Serres, X. Mateos, W. Zhou, D. Shen, U. Griebner, V. Petrov, 67-fs pulse generation from a mode-locked Tm,Ho:CLNGG laser at 2083 nm, Opt. Express 27 (2019) 1922-1928.
15. Y.-J. Shen, B.-Q. Yao, X.-M. Duan, G.-L. Zhu, W. Wang, Y.-L. Ju, Y.-Z. Wang, 103 W in-band dual-end-pumped Ho:YAG laser, Opt. Lett. 37 (2012) 3558-3560.
16. K. Shimamura, M. Timoshechkin, T. Sasaki, K. Hoshikawa, T. Fukuda, Growth and characterization of calcium niobium gallium garnet (CNGG) single crystals for laser applications, J. Cryst. Growth 128 (1993) 1021-1024.
17. P. A. Ryabochkina, A. N. Chabushkin, N. G. E. Zakharov, K. V. E. Vorontsov, S. A. Khrushchalina, Tunable 2-μm lasing in calcium–niobium–gallium garnet crystals doped with Ho^{3+} ions, Quantum Electron. 47 (2017) 607-609.
18. Y. Xue, N. Li, Q. Song, X. Xu, X. Yang, T. Dai, D. Wang, Q. Wang, D. Li, Z. Wang, J. Xu, Spectral properties and laser performance of Ho:CNGG crystals grown by the micro-pulling-down method, Opt. Mater. Express 9 (2019) 2490-2496.
19. R. Wälti, W. Lüthy, H.P. Weber, S.Y. Rusanow, A.A. Yakovlev, A.I. Zagumenyi, I. Shcherbakov, A.F. Umyskov, Yb^{3+} Ho^{3+} energy exchange mechanisms in Yb: Ho: YAG crystals for 2 μm or 540 nm lasing, J. Quant. Spectrosc. Radiat. Transf. 54 (1995) 671-681.
20. T. Rothacher, W. Lüthy, H.P. Weber, Diode pumping and laser properties of Yb: Ho: YAG, Opt. Commun. 155 (1998) 68-72.
21. A. Diening, S. Kück, Spectroscopy and diode-pumped laser oscillation of Yb^{3+}, Ho^{3+}-doped yttrium scandium gallium garnet, J. Appl. Phys. 87 (2000) 4063-4068.
22. V.M. Gordienko, F.V. Potemkin, A.V. Pushkin, A.A. Sirotkin, V.V. Firsov, Powerful 3 μm YSGG: Cr: Er and YSGG: Cr: Yb: Ho Q-switched lasers operating in the repetition-rate mode, J. Russ. Laser Res. 36 (2015) 570-576.
23. S.D. Jackson, S. Mossman, Diode-cladding-pumped Yb^{3+}, Ho^{3+}-doped silica fiber laser operating at 2.1-μm, Appl. Opt. 42 (2003) 3546-3549.
24. J. Li, D.D. Hudson, S.D. Jackson, High-power diode-pumped fiber laser operating at 3 μm, Opt. Lett. 36 (2011) 3642-3644.

25. L. Wetenkamp, Efficient CW operation of a 2.9 μm Ho^{3+}-doped fluorozirconate fibre laser pumped at 640 nm, Electron. Lett. 26 (1990) 883-884.
26. A. Braud, S. Girard, J.L. Doualan, R. Moncorge, Spectroscopy and fluorescence dynamics of (Tm^{3+}, Tb^{3+}) and (Tm^{3+}, Eu^{3+}) doped $LiYF_4$ single crystals for 1.5-μm laser operation, IEEE J. Quantum Electron. 34 (1998) 2246-2255.
27. Y. Zhou, J. Chen, L. Dong, S. Cao, Y. Zhang, W. Han, H. Xu, J. Liu, Growth and spectroscopic properties of Yb–Ho co-doped CNGG crystal, Opt. Mater. 114 (2021) 110998.
28. W. T. Carnall, P. R. Fields, K. Rajnak, Electronic energy levels in the trivalent lanthanide aquo ions. I. Pr^{3+}, Nd^{3+}, Pm^{3+}, Sm^{3+}, Dy^{3+}, Ho^{3+}, Er^{3+}, and Tm^{3+}, J. Chem. Phys. 49 (1968) 4424-4442.
29. Yu.K. Voron'ko, N. Es'kov, Luminescence of Eu^{3+} activator centres in calcium-niobium-gallium garnet crystals, Inorg. Mater. 30 (1994) 100-104.
30. B. Aull, H. Jenssen, Vibronic interactions in Nd:YAG resulting in nonreciprocity of absorption and stimulated emission cross sections, IEEE J. Quantum Electron. 18 (1982) 925-930.
31. S. A. Payne, L. L. Chase, L. K. Smith, W. L. Kway, W. F. Krupke, Infrared cross-section measurements for crystals doped with Er^{3+}, Tm^{3+} and Ho^{3+}, IEEE J. Quantum Electron. 28 (1992) 2619–2630.
32. J.B. Gruber, G.W. Burdick, U.V. Valiev, K.L. Nash, S.A. Rakhimov, D.K. Sardar, Energy levels and symmetry assignments for Stark components of $Ho^{3+}(4f^{10})$ in yttrium gallium garnet ($Y_3Ga_5O_{12}$), J. Appl. Phys. 106 (2009) 113110.
33. P.A. Loiko, G.E. Rachkovskaya, G.B. Zakharevich, A.A. Kornienko, E.B. Dunina, A.S. Yasukevich, K.V. Yumashev, Cooperative up-conversion in Eu^{3+}, Yb^{3+}-doped SiO_2–PbO–PbF_2–CdF_2 oxyfluoride glass, J. Non-Cryst. Solids 392 (2014) 39-44.

Table 1. Initial (C_{melt}) and actual ($C_{crystal}$) doping concentrations of rare-earth ions and their segregation coefficients (K_{RE}) for the studied Yb,Ho:CNGG and Yb,Ho,Eu:CNGG crystals.

C_{melt}, at.%			$C_{crystal}$, at.%		K_{RE}	
Yb	Ho	Eu	Yb	Ho	K_{Yb}	K_{Ho}
10	0.075	-	11.5	0.94	1.15	1.25
10	0.075	0.2	11.5	0.94	1.15	1.25
10	1	-	11.5	1.25	1.15	1.25
10	1	0.075	11.5	1.25	1.15	1.25
10	1	0.2	11.5	1.25	1.15	1.25

Table 2. Fractional atomic coordinates (*x*, *y*, *z*), occupancy factors (O.F.) and isotropic displacement parameters (B_{iso}) for the Yb,Ho,Eu:CNGG crystal.

Atom	Wyckoff	*x*	*y*	*z*	O.F.	B_{iso}, Å^2
Ca	24*c*	0.1250(0)	0.0000	0.2500(0)	0.872	1.675(0)
Yb	24*c*	0.1250(0)	0.0000	0.2500(0)	0.115	1.675(0)
Ho|Eu	24*c*	0.1250(0)	0.0000	0.2500(0)	0.012|0.001	1.675(0)
Ga1	16*a*	0.0000	0.0000	0.0000	0.3000	0.388(4)
Nb1	16*a*	0.0000	0.0000	0.0000	0.6900	0.388(4)
Nb2	24*d*	0.3750(0)	0.0000	0.2500(0)	0.0970	0.596(0)
Ga2	24*d*	0.3750(0)	0.0000	0.2500(0)	0.9091	0.596(0)
O	96*h*	0.4483(0)	0.1485(4)	1.0294(0)	1.0000	1.851(0)

Table 3. Measured luminescence lifetimes τ_{lum} of selected excited-states of Yb^{3+}, Ho^{3+} and Eu^{3+} ions in CNGG crystals.

Concentration, at.%			τ_{lum}, ms			
Yb	Ho	Eu	Yb ($^2F_{5/2}$)	Ho ($^5I_6$)	Ho ($^5I_7$)	Eu ($^5D_0$)
11.9	-	-	0.978	-	-	-
11.5	0.94	-	0.805	0.304	7.242	-
11.5	1.25	-	0.523	0.294	7.244	-
11.5	0.94	0.2	0.744	0.295	3.683	0.918
11.5	1.25	0.075	0.633	0.276	4.215	0.914
11.5	1.25	0.2	0.569	0.273	3.238	0.899

Table 4. Energies of Stark sub-levels of the $^5I_8$, $^5I_7$ and $^5I_6$ Ho^{3+} multiplets in CNGG.

Multiplet	Energy, cm^{-1}
$^5I_8$	0; 15; 55; 73; 90; 103; 110; 368; 382; 389; 401; 418; 434; 447; 461; 485 (*1 missing*)
$^5I_7$	5408; 5385; 5376; 5348; 5328; 5311; 5283; 5252; 5206; 5214; 5211; 5208 (*3 missing*)
$^5I_6$	8913; 8881; 8865; 8842; 8826; 8818; 8811; 8780; 8741; 8711 (*3 missing*)

List of figures

Figure 1. A photograph of an as-grown Yb,Ho,Eu:CNGG crystal (11.5 at.% Yb^{3+}, 1.25 at.% Ho^{3+}, 0.075 at.% Eu^{3+}), the growth direction is along the [111] axis.

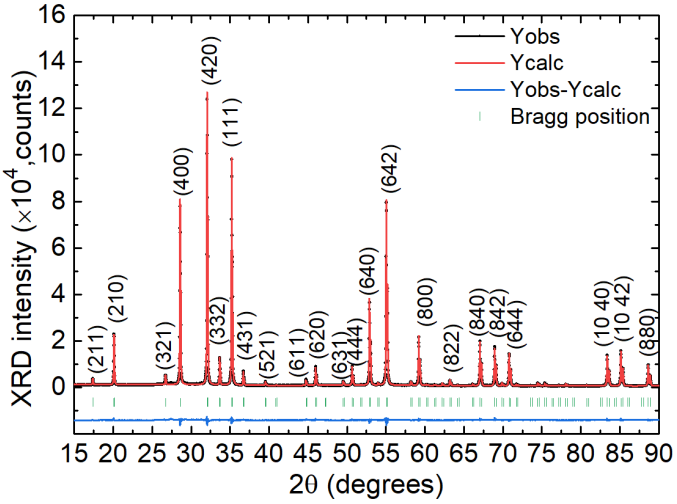

Figure 2. Rietveld structure refinement of the XRD pattern of the Yb,Ho,Eu:CNGG crystal (11.5 at.% Yb^{3+}, 1.25 at.% Ho^{3+}, 0.075 at.% Eu^{3+}): measured (Y_{obs}, *black*), calculated (Y_{calc}, *red*) and residual ($Y_{obs} - Y_{calc}$, *blue*) patterns, *green dashes* – Bragg reflections, *numbers* denote the Miller's indices, (*hkl*).

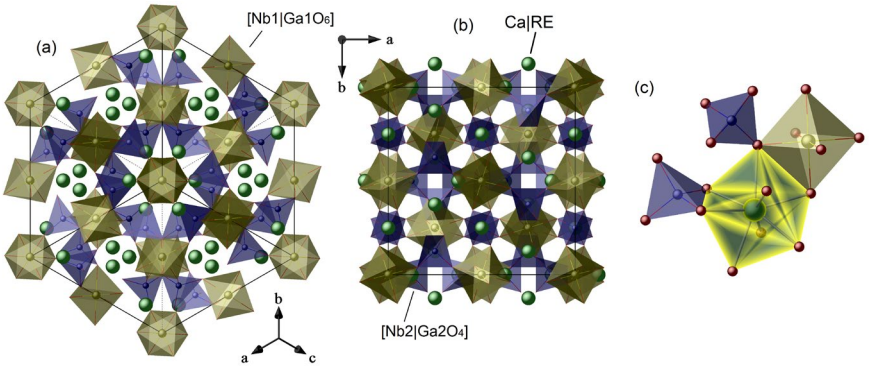

Figure 3. Crystal structure of Yb,Ho,Eu:CNGG: (a) [111] view; (b) a projection on the ***a*-*b*** crystallographic plane; (c) the connection between the polyhedra [Ca|REO_8], [Nb1|$Ga1O_6$] and [Nb2|$Ga2O_4$].

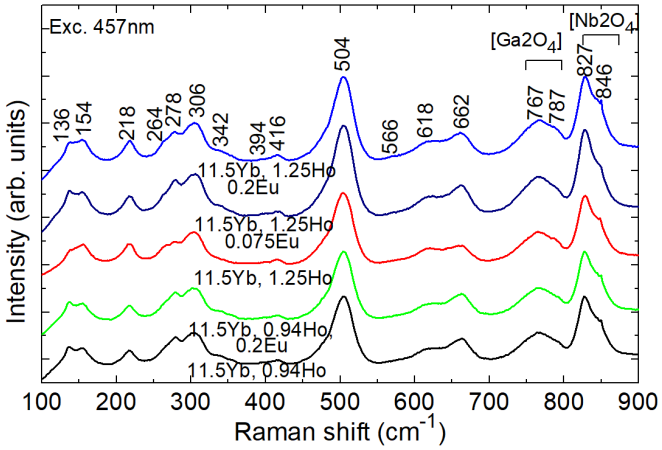

Figure 4. Unpolarized Raman spectra of Yb,Ho: and Yb,Ho,Eu:CNGG crystals, *numbers* denote the phonon energies in cm^{-1}, λ_{exc} = 457 nm.

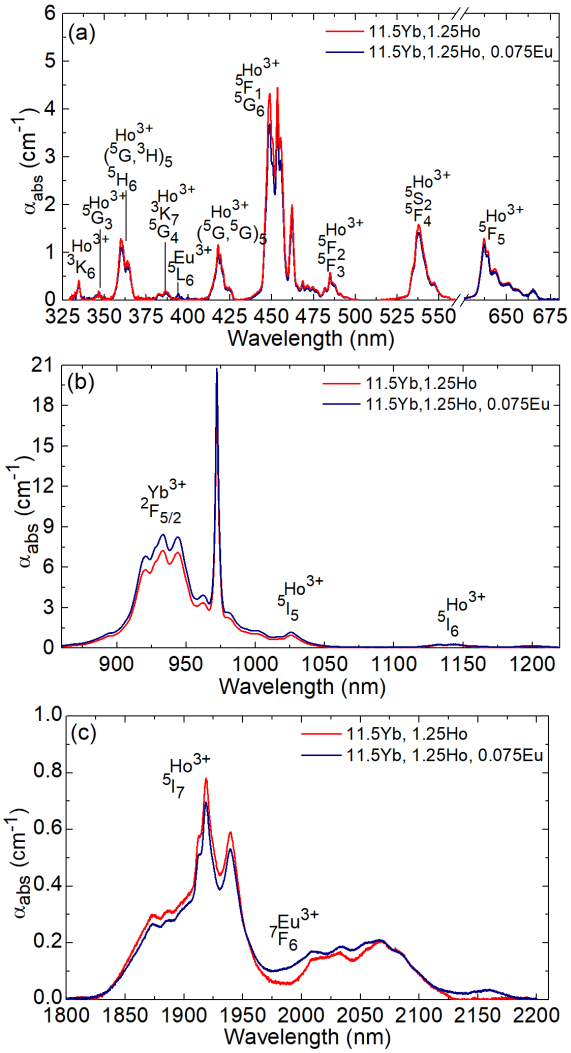

Figure 5. RT absorption spectra of Yb,Ho: and Yb,Ho,Eu:CNGG crystals: spectral range (a) 325–680 nm, (b) 860–1220 nm, (c) 1800–2200 nm.

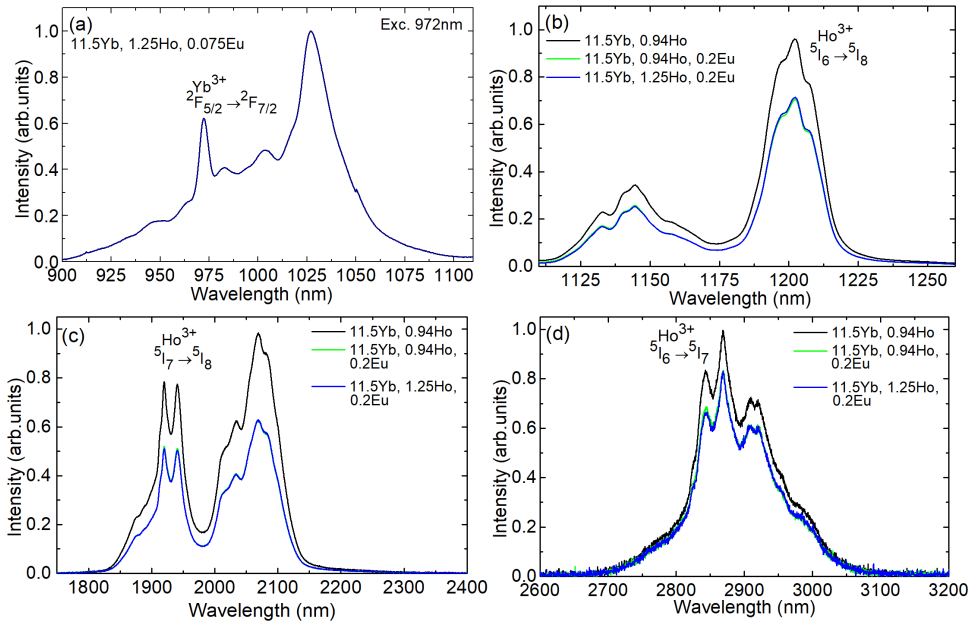

Figure 6. RT luminescence spectra of Yb,Ho: and Yb,Ho,Eu:CNGG crystals: (a) Yb^{3+} ions, the $^5F_{5/2} \rightarrow {}^5F_{7/2}$ transition, (b) Ho^{3+} ions, the $^5I_6 \rightarrow {}^5I_8$ transition, (c) Ho^{3+} ions, the $^5I_7 \rightarrow {}^5I_8$ transition, (d) Ho^{3+} ions, the $^5I_6 \rightarrow {}^5I_7$ transition, $\lambda_{exc} = 972.1$ nm.

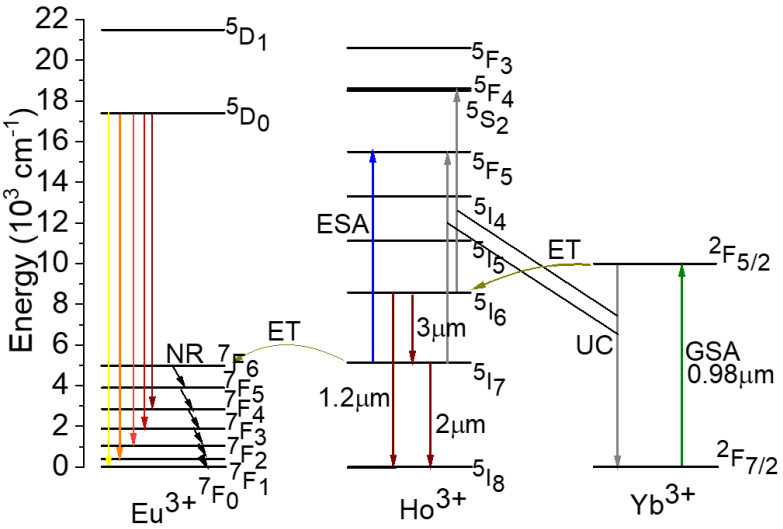

Figure 7. A simplified scheme of energy-levels of Yb^{3+}, Ho^{3+} and Eu^{3+} ions showing different spectroscopic processes: ET – energy-transfer, GSA and ESA – ground-state and excitation-state absorption, respectively, NR – non-radiative transitions, UC – upconversion.

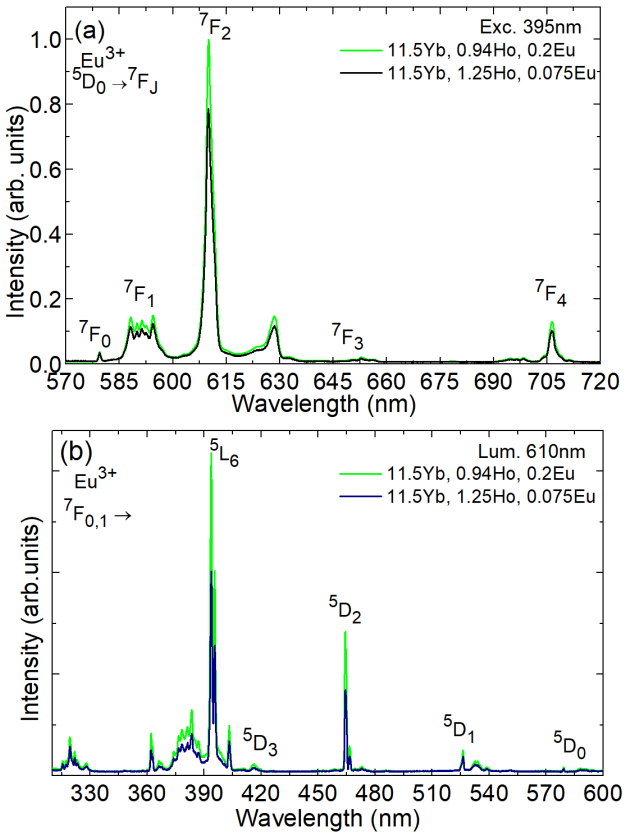

Figure 8. (a) Luminescence (λ_{exc} = 395 nm) and (b) excitation (λ_{lum} = 610 nm) spectra of Eu^{3+} ions in Yb,Ho,Eu:CNGG crystals at RT.

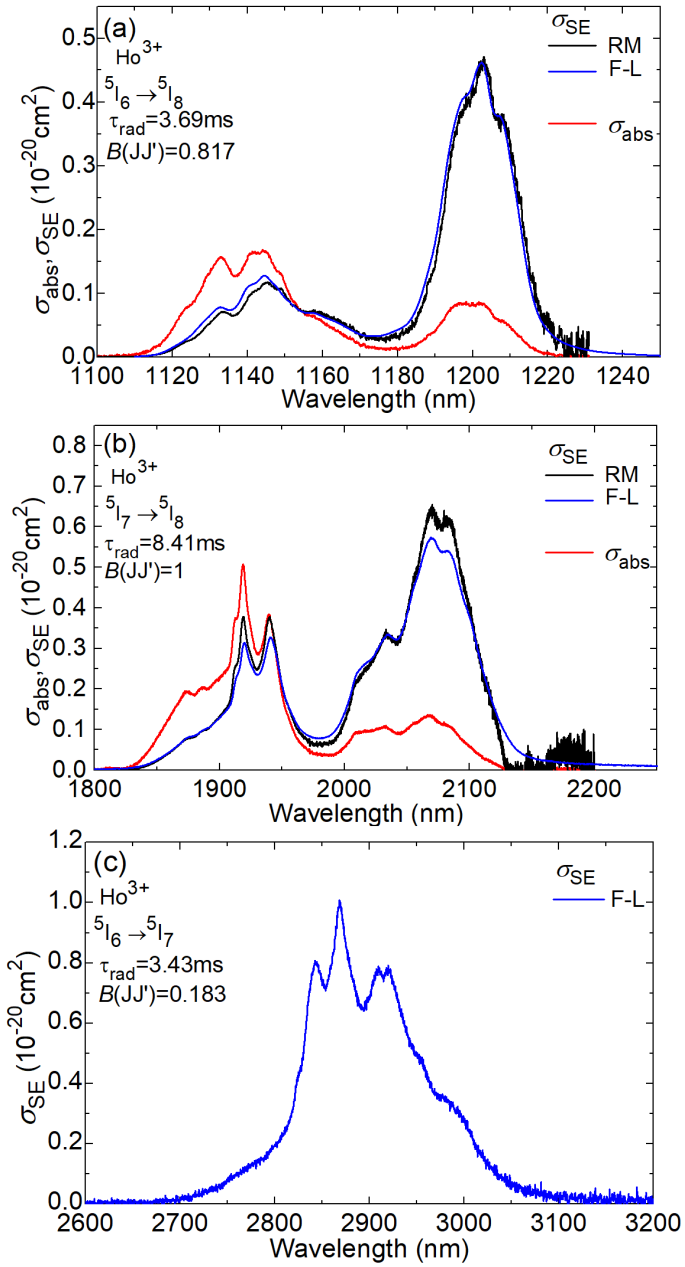

Figure 9. RT transition cross-section of Ho^{3+} ions in the CNGG crystal: (a,b) absorption, σ_{abs}, and stimulated-emission (SE), σ_{SE}, cross-sections, for the (a) $^5I_6 \rightarrow {}^5I_8$ and (b) $^5I_7 \rightarrow {}^5I_8$ transitions; (c) SE cross-sections, σ_{SE}, for the $^5I_6 \rightarrow {}^5I_7$ transition. RM - reciprocity method, F-L - Füchtbauer-Ladenburg formula, τ_{rad} – radiative lifetime of the emitting state, B(JJ') – luminescence branching ratio [12].

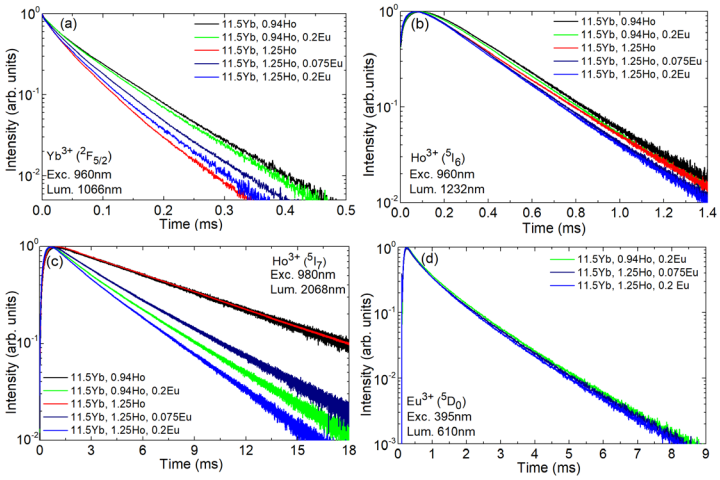

Figure 10. RT luminescence decay curves for Yb^{3+}, Ho^{3+} and Eu^{3+} ions in the CNGG crystals: (a) the $^2F_{5/2}$ Yb^{3+} state, $\lambda_{exc} = 960$ nm, $\lambda_{lum} = 1066$ nm, (b) the $^5I_6$ Ho^{3+} state, $\lambda_{exc} = 960$ nm, $\lambda_{lum} = 1232$ nm, (c) the $^5I_7$ Ho^{3+} state, $\lambda_{exc} = 980$ nm, $\lambda_{lum} = 2068$ nm and (d) the $^5D_0$ Eu^{3+} state, $\lambda_{exc} = 395$ nm, $\lambda_{lum} = 610$ nm.

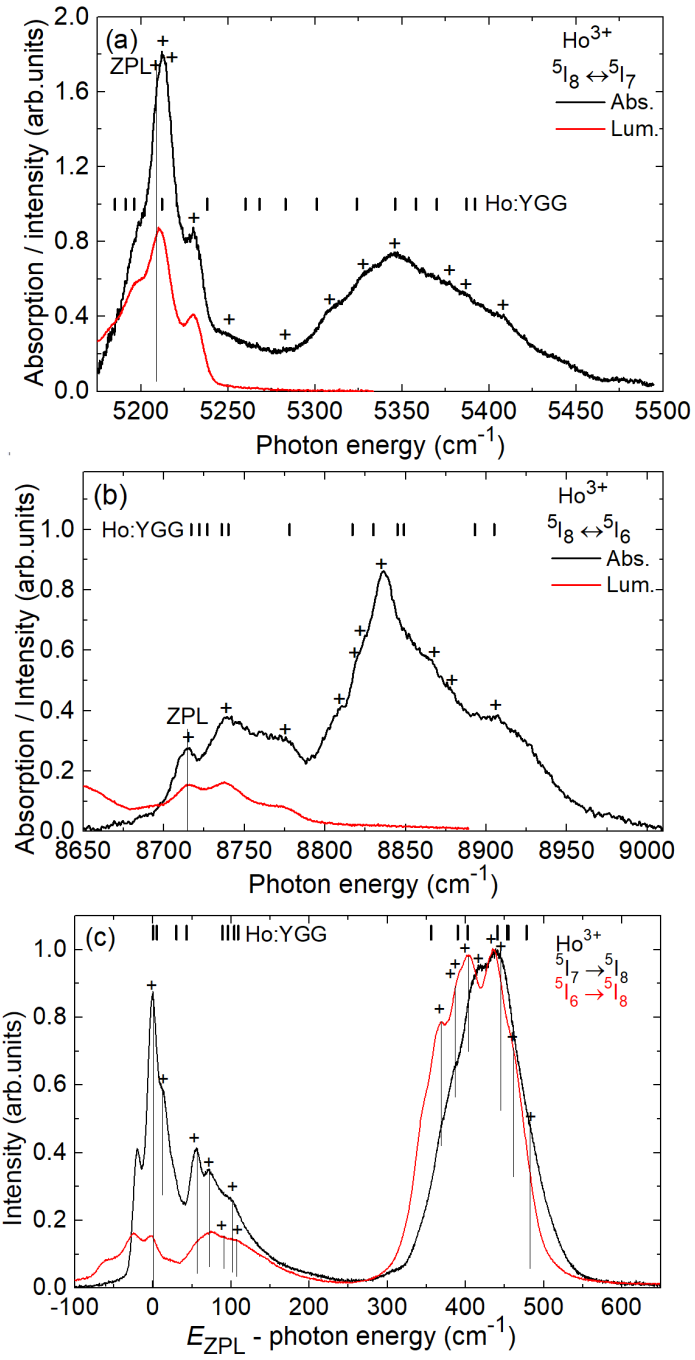

Figure 11. Low-temperature (LT, 12 K) spectroscopy of Ho^{3+} ions in the CNGG crystal: (a,b) absorption spectra: the $^5I_8 \rightarrow {}^5I_7$ transition; (b) the $^5I_8 \rightarrow {}^5I_6$ transition; (c) luminescence spectra, the $^5I_7 \rightarrow {}^5I_8$ and the $^5I_6 \rightarrow {}^5I_8$ transitions, ZPL – zero-phonon-lines, "+" indicate the assigned electronic transitions, *vertical dashes* – crystal-field splitting for Ho^{3+} ions in the YGG crystal [32].

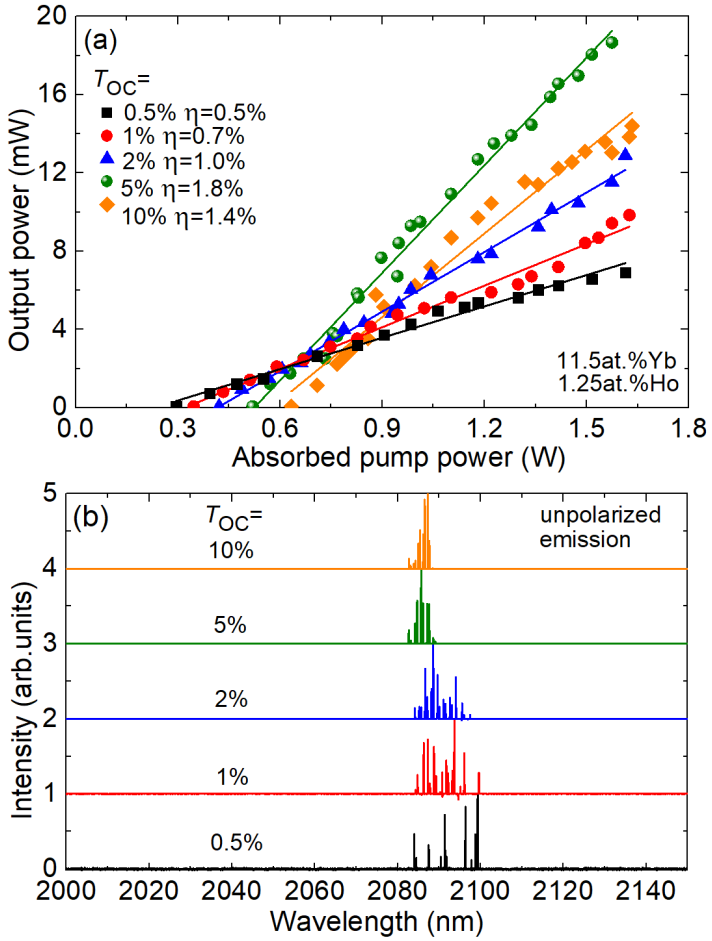

Figure 12. Yb,Ho:CNGG laser operating on the $^5I_7 \rightarrow {}^5I_8$ Ho^{3+} transition: (a) input-output dependences, η – slope efficiency; (b) typical spectra of unpolarized laser emission. 11.5 at.% Yb^{3+}, 1.25 at.% Ho^{3+}:CNGG crystal, pump wavelength: 950 nm.